nature portfolio

https://doi.org/10.1038/s41551-021-00764-3

Supplementary information

Reduction of choroidal neovascularization via cleavable VEGF antibodies conjugated to exosomes derived from regulatory T cells

In the format provided by the authors and unedited

Supplementary information

Content

aV from rEXS

Supplementary Fig. 14. Detection of leakage numbers after different treatments in CNV mouse and monkey models

Supplementary Fig. 15. Side effect evaluation *via* detection of hematological parameter in a CNV mouse model

Supplementary Fig. 16. H&E staining of heart, liver, spleen, lung, and kidney slices after treatment with rEXS-cL-aV in a CNV mouse model

Supplementary Fig. 17. Hematological parameters detection in a CNV monkey model

Supplementary Fig. 18. Flow cytometry gating strategy for Fig. 3c

Supplementary Fig. 19. Flow cytometry gating strategy for Fig. 3e

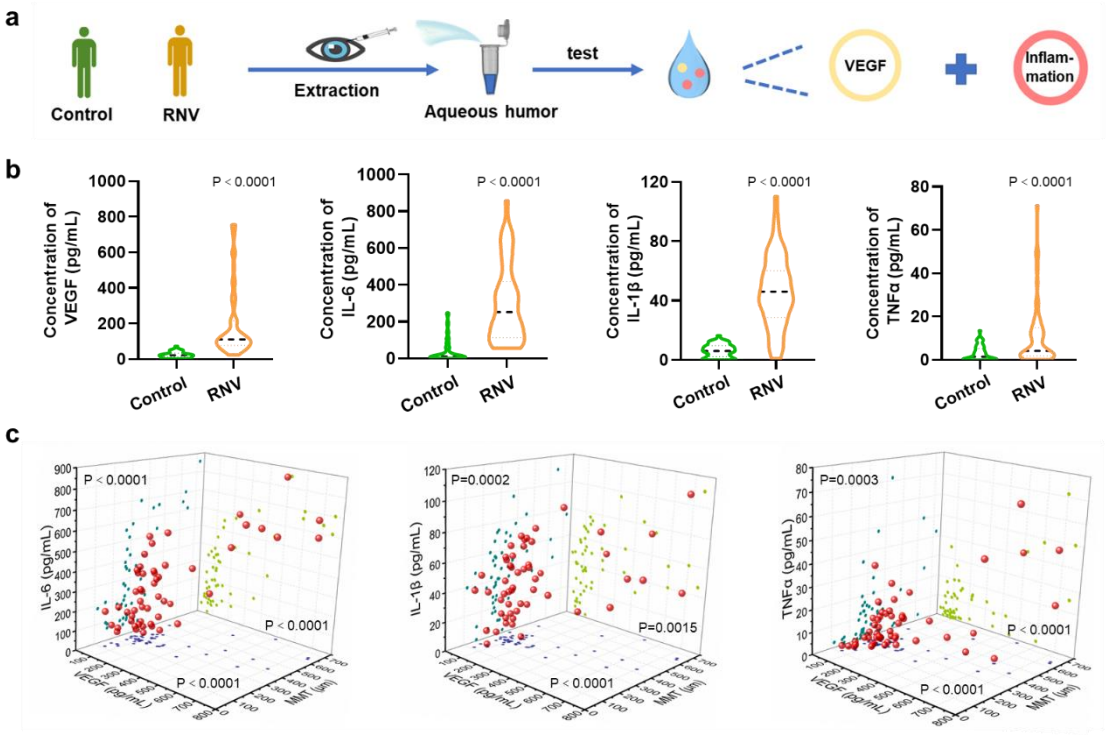

Supplementary Fig. 1. The levels of neovascularization-related factors and inflammatory cytokines in aqueous humor of RNV patients

a, Schematic for the extraction of aqueous humor, and its following tests of VEGF and inflammatory cytokines in Control and RNV groups. Control: patients with age-related cataract without ocular neovascular diseases (n=50); RNV: patients with retinal neovascularization. **b**, The levels of VEGF, IL-6, IL-1β, and TNFα in aqueous humor of RNV patients (n=52). **c**, Red dots represented for correlation analyses of relationships among VEGF, MMT and inflammatory cytokines (IL-6, IL-1β or TNFα) in RNV patients. XY plane (purple dots) represented for correlation between VEGF and MMT. XZ plane (green dots) represented for correlation between VEGF and inflammatory cytokines. YZ plane (blue dots) represented for correlation between MMT and inflammatory cytokines. Strong positive correlations were observed between the levels of pro-inflammatory cytokines and VEGF. MMT correlated with VEGF and pro-inflammatory cytokines, especially IL-

6 and IL-1β. Comparable upregulation of pro-inflammatory cytokines also correlated with MMT. Data in b were presented as the mean ± SEM, and were measured by two-tailed unpaired Student' s *t*-test. Data in c was measured by regression analysis.

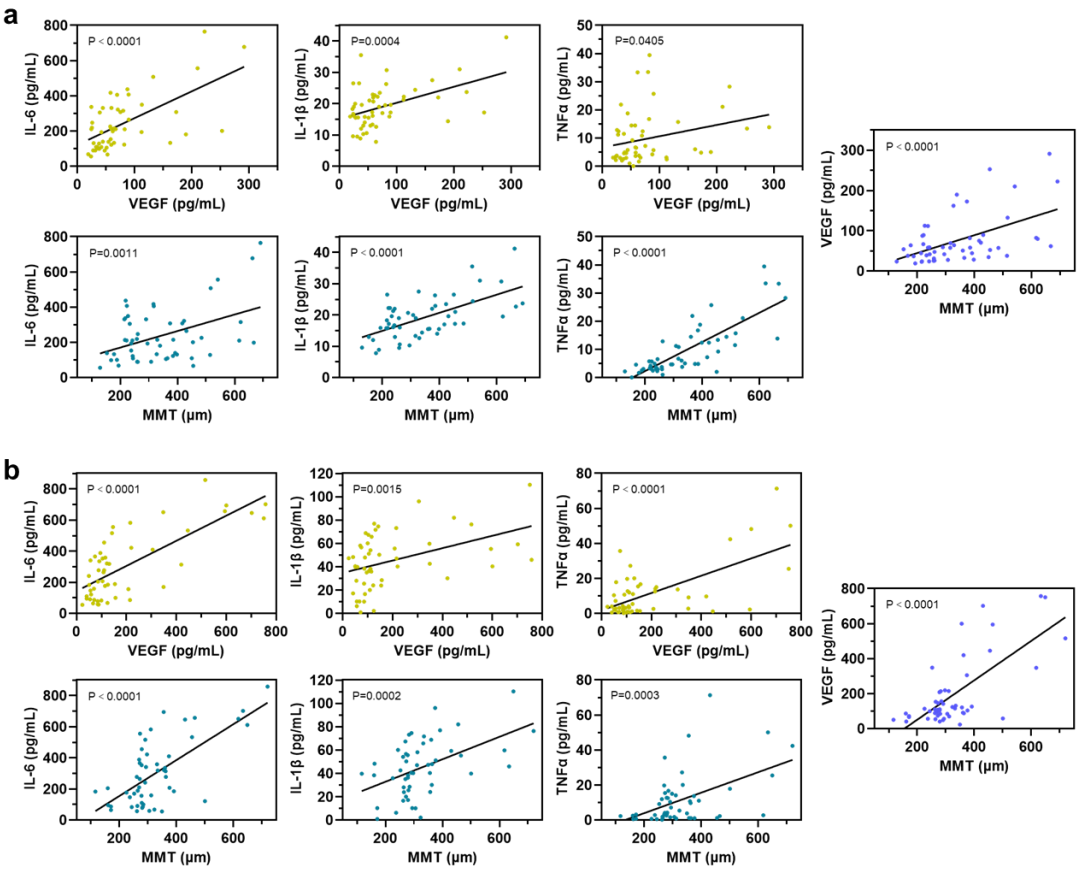

Supplementary Fig. 2. Correlations among inflammatory cytokines (IL-6, IL-1β or TNFα), VEGF and MMT in patients by 2D graph for Fig. 1c and Supplementary Fig. 1c

Correlation analyses in IL-6 vs VEGF, IL-1β vs VEGF, TNFα vs VEGF, IL-6 vs MMT, IL-1β vs MMT, TNFα vs MMT, VEGF vs MMT in 53 CNV patients (**a**) and in 52 RNV patients (**b**). Strong positive correlations were observed in either two aspects of inflammatory cytokines, VEGF, and MMT in both CNV and RNV patients. Data in a and b were measured by regression analysis.

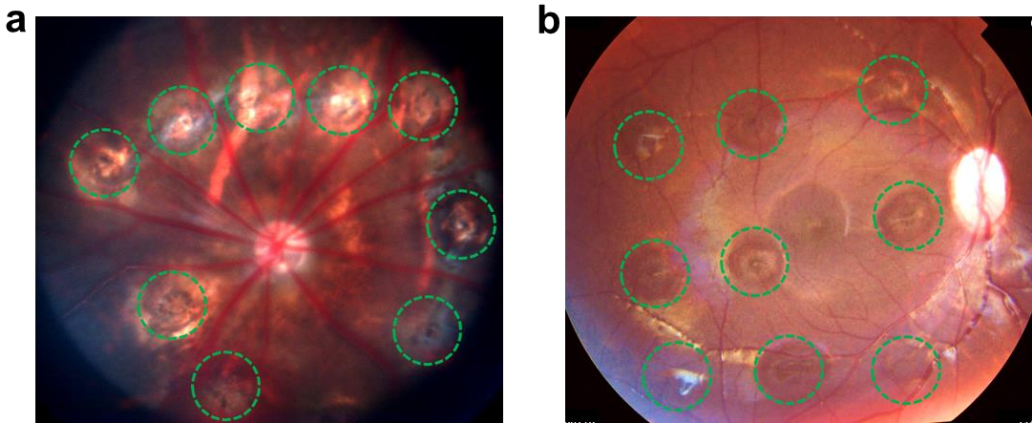

Supplementary Fig. 3. The ocular fundus photograph of laser-induced CNV models

a, Representative ocular fundus with choroidal neovascularization lesions in the CNV mouse model (C57BL/6, 3 days after treating with laser photocoagulation). **b**, Representative ocular fundus with choroidal neovascularization lesions in the CNV monkey model (cynomolgus monkeys, 7 days after treating with laser photocoagulation). The green circles indicated the CNV lesions, which were successfully induced by laser photocoagulation.

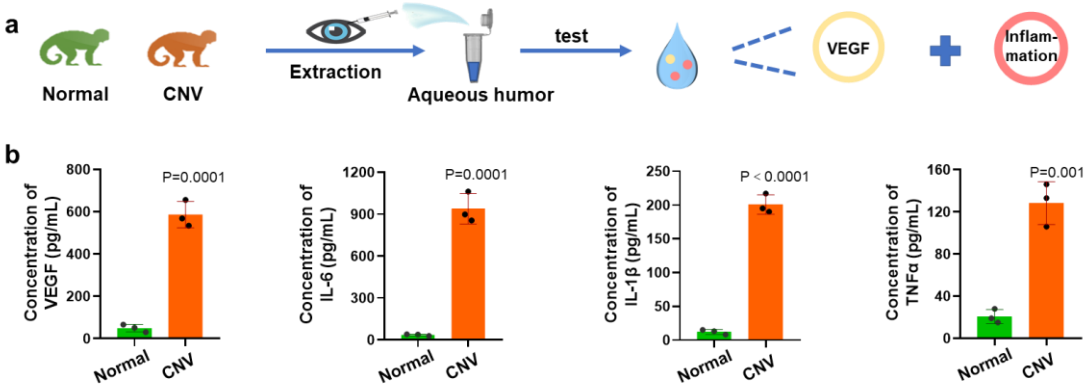

Supplementary Fig. 4. Co-morbidity of VEGF and inflammation in a CNV monkey model

a, Schematic for testing VEGF and inflammatory cytokines in aqueous humor of the CNV cynomolgus monkey model. **b**, The levels of VEGF, IL-6, IL-1β and TNFα in aqueous humor of the CNV cynomolgus monkey model. For quantitation, aqueous humor was detected in 1 eye from each of 3 monkeys (n=3). Data in b were presented as the mean ± SEM, and were measured by two-tailed unpaired Student's *t*-test.

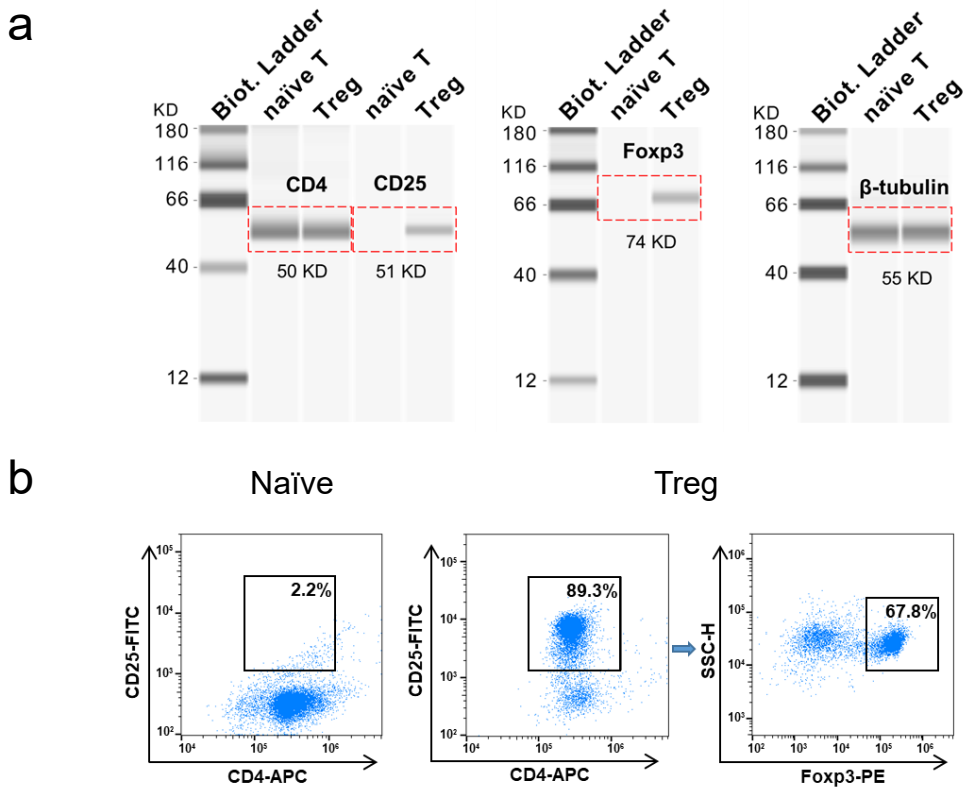

Supplementary Fig. 5. Identification of naïve CD4$^+$ T cells and Treg cells before and after induction

a, Western blotting analysis of CD4, CD25 and Foxp3 in naïve CD4$^+$ T and Treg cells by ProteinSimple Wes^{TM} Capillary Western Blot analyzer. β-tubulin was used as housekeeping protein normalizing the levels of protein. Both naïve CD4$^+$ T cells and Treg cells expressed high levels of CD4, while the expressions of CD25 and Foxp3 were only observed for Treg cells. **b**, Flow cytometry analysis of naïve CD4$^+$ T cells and Treg cells (Foxp3$^+$ gating on CD4$^+$ CD25$^+$ T cells). The proportion of Treg cells raised significantly after 7 days-induction from naïve CD4$^+$ T cells.

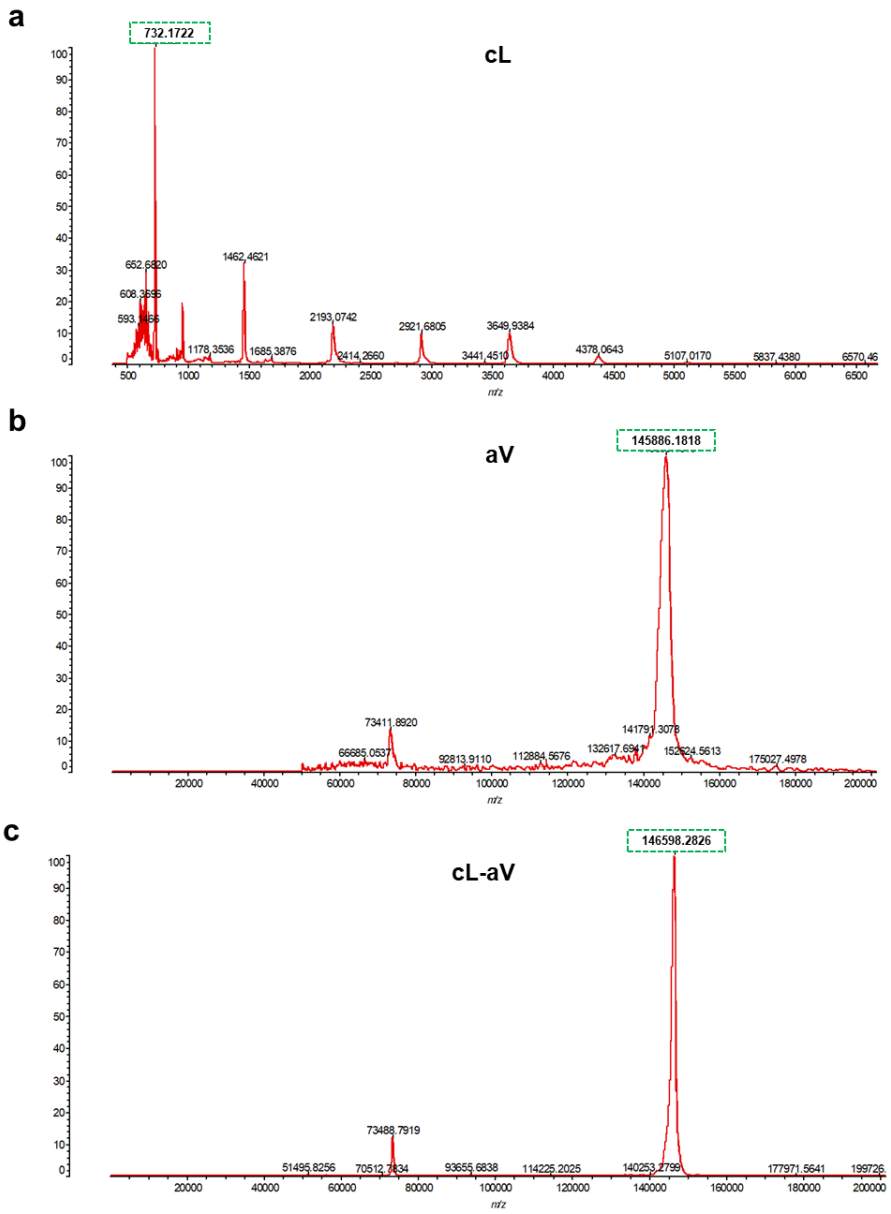

Supplementary Fig. 6. MALDI/TOF spectra analysis for the cleavable linker (cL) modification of the anti-VEGF antibody

a, Spectra indicated the relative molecular weight of a cleavable linker (cL) (732.1722). **b**, Spectra indicated the relative molecular weight of anti-VEGF antibody (aV) (145886.1818). **c**, Peak in 146598.2826 came from the cL and av, suggesting the successful conjugation of cL and aV.

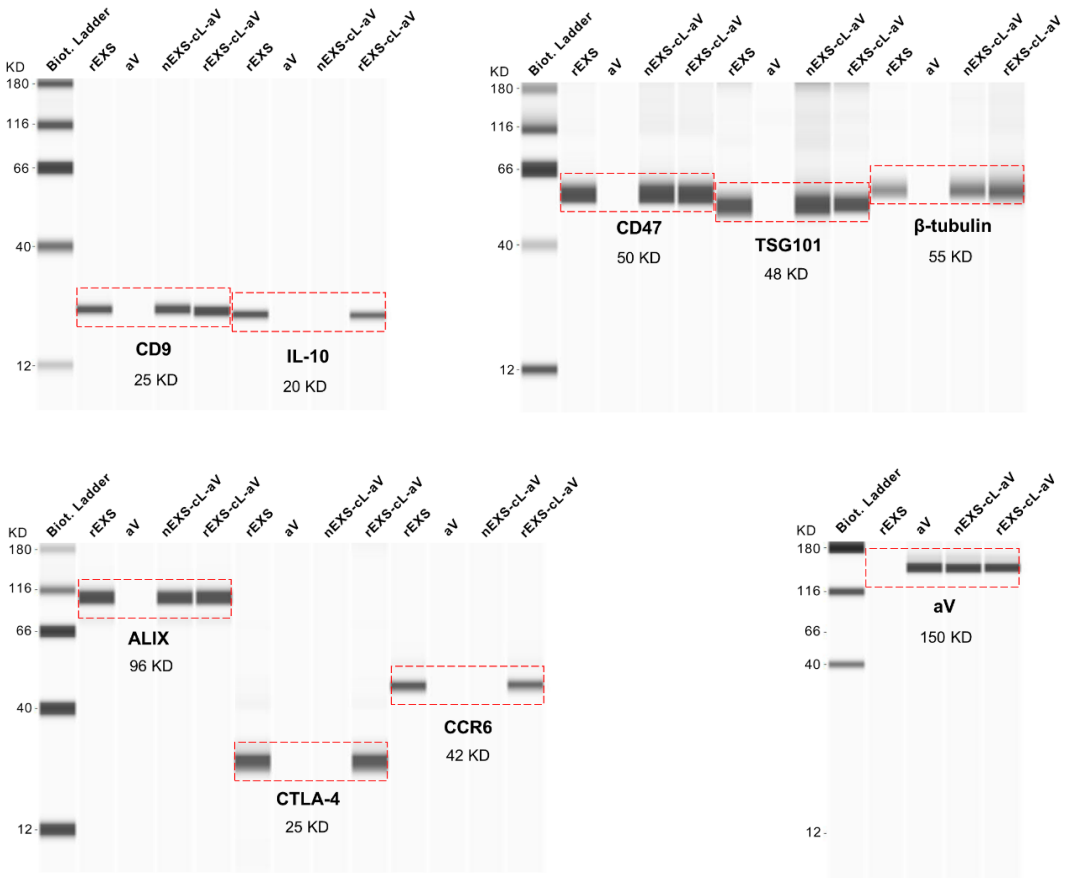

Supplementary Fig. 7. The full scans of Fig. 2f

Western blotting analysis of rEXS, aV, nEXS-cL-aV (nEXS, exosomes from naïve $CD4^+$ T cells) and rEXS-cL-aV by ProteinSimple Wes™ Capillary Western Blot analyzer.

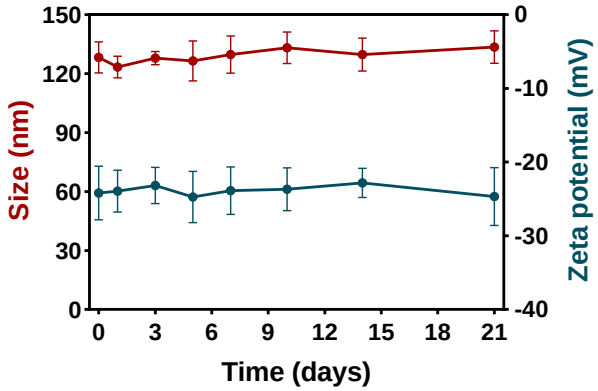

Supplementary Fig. 8. Hydrodynamic sizes and zeta potentials of rEXS-cL-aV during storage in PBS at 4 ℃

The values of size and zeta potential showed very slight fluctuations during storage over three weeks. Data were presented as the mean ± SEM (n=3 biologically independent samples).

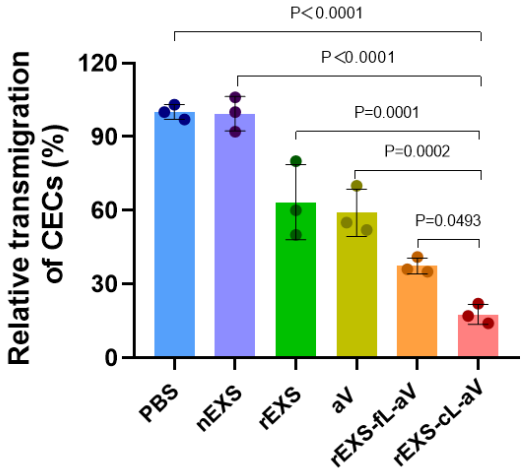

Supplementary Fig. 9. Quantitative analysis of relative transmigration of CECs in Figure 3b

Relative transmigration of CECs: the ratio of density of CECs on the back of the upper chamber exposed to nEXS, rEXS, aV, rEXS-fL-aV or rEXS-cL-aV to that exposed to PBS (n=3 biologically independent experiments). Data were presented as the mean ± SEM, and were measured by one-way ANOVA.

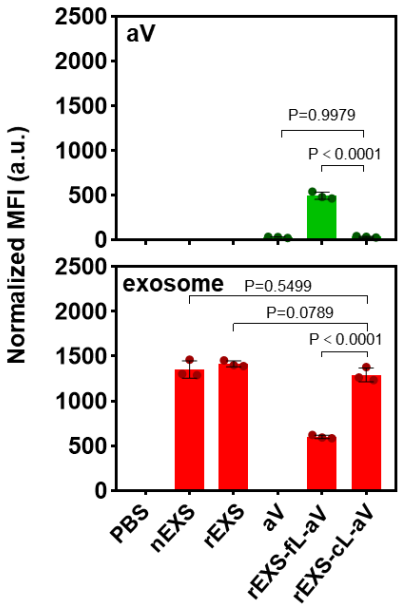

Supplementary Fig. 10. Quantitative analysis of normalized fluorescence intensity of aV and rEXS in Fig. 3d

The rEXS-fL-aV led to the consumption of aV in macrophages, which was reduced in macrophages for the cleavable linker in rEXS-cL-aV group. MFI: mean fluorescence intensity. Data were presented as the mean ± SEM, and were measured by one-way ANOVA (n=3 biologically independent experiments).

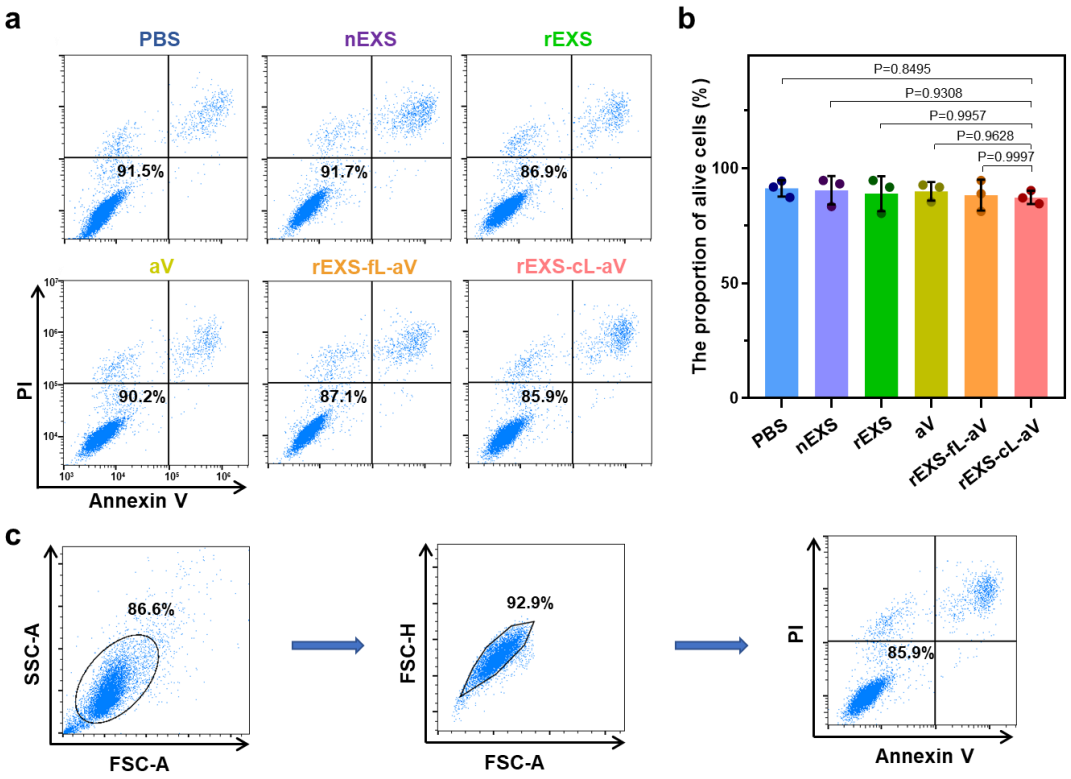

Supplementary Fig. 11. Detection the survival of macrophages from lower chamber

a, Flow cytometry analysis of activated macrophages by the Annexin V/PI detection. **b**, The proportion of live cells with different samples in a (n=3 biologically independent experiments). Compared with the PBS group, other groups (including nEXS, rEXS, aV, rEXS-fL-aV, and rEXS-cL-aV) showed a comparable high proportion of live cells, thus excluding the influence of cell variation on the CD86 expression level. **c**, Flow cytometry gating strategy for a. Data in b were presented as the mean ± SEM, and were measured by one-way ANOVA.

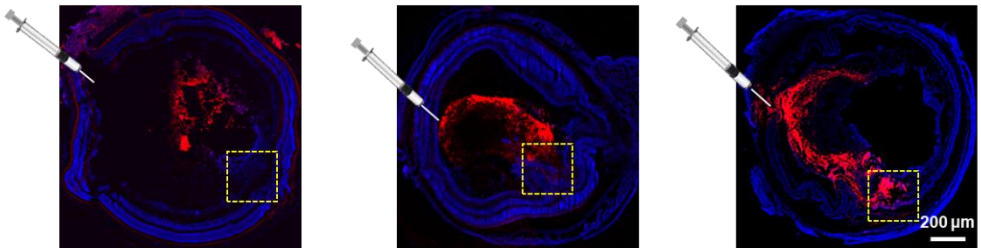

Supplementary Fig. 12. Intravitreal distribution of aV in a CNV mouse model

The rEXS-based nanodrugs could be attracted from the anterior segment to the posterior segment of eyeballs upon the concentration gradient of inflammatory cytokines from CNV lesions to injection site. Therefore, aV conjugated on rEXS-based nanodrugs (rEXS-fL-aV or rEXS-cL-aV) showed accumulation to the CNV lesions.

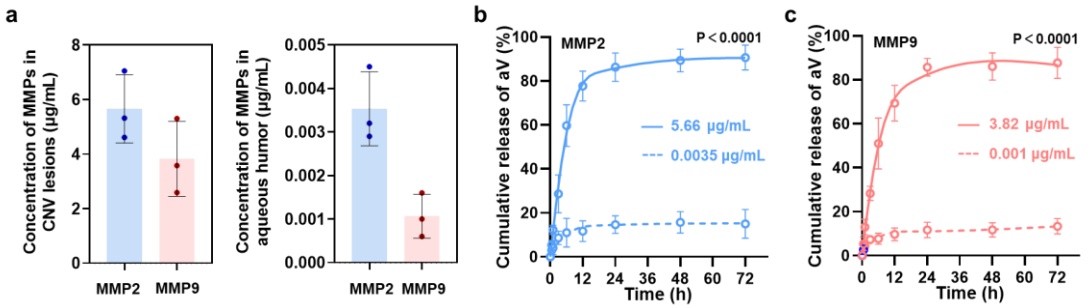

Supplementary Fig. 13. *In vivo* concentrations of MMP2 and MMP9 for triggering the cleavage of aV from rEXS

a, Detection of MMP2 and MMP9 concentrations at CNV lesion and in aqueous humor by ELISA assay. Each sample was harvested from 6 eyes of 6 mice, and 3 samples (n=3 biologically independent samples) were used for calculation in each group. **b**, ELISA-based quantification of aV levels from cleavage of rEXS-cL-aV under 5.66 μg/mL (concentration at lesion) and 0.0035 μg/mL (concentration in aqueous humor) MMP2 for comparison (n=3 biologically independent experiments). **c**, Quantification of aV levels from cleavage of rEXS-cL-aV under 3.82 μg/mL (concentration of lesion) and 0.001 μg/mL (concentration in aqueous humor) MMP9 for comparison (n=3 biologically independent experiments). The significant difference (>1,000 folds) of MMP concentrations between the lesion and aqueous humor ensured the cleavage could specifically occur in the lesion site. Data in a, b and c were presented as the mean ± SEM, and data in b and c were measured by two-tailed unpaired Student' s *t*-test.

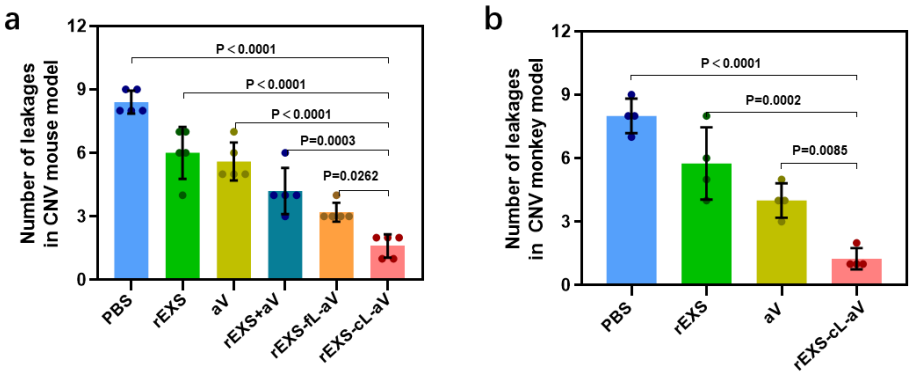

Supplementary Fig. 14. Detection of leakage numbers after different treatments in CNV mouse and monkey models

a, Quantification of leakage numbers after different treatments in the mouse model of Fig. 5d. For calculation, 1 eye was detected from each of 5 mice (n=5). **b**, Quantification of leakage numbers after different treatments in the monkey model of Fig. 6c. For calculation, 1 eye was detected from each of 4 monkeys (n=4). The treatment of rEXS-cL-aV drastically reduced the number of leakage and outperformed all other groups in both CNV mouse and monkey models. Data in a and b were presented as the mean ± SEM, and were measured by one-way ANOVA.

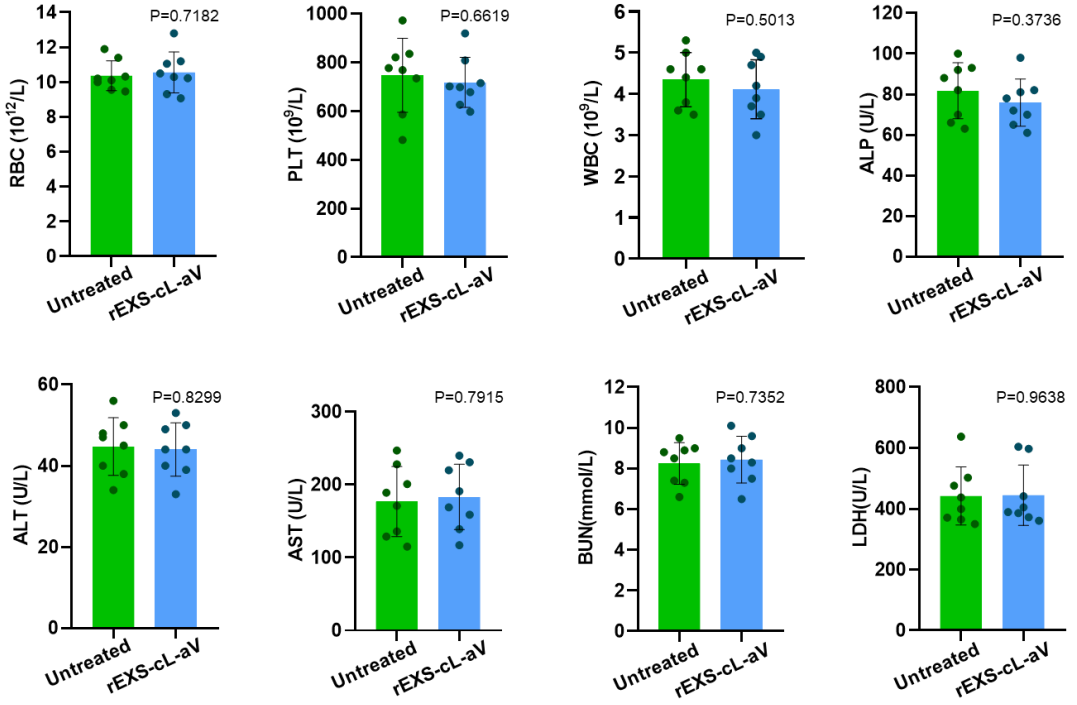

Supplementary Fig. 15. Side effect evaluation *via* detection of hematological parameter in a CNV mouse model

The red blood cell (RBC), platelet (PLT), white blood cell (WBC), alkaline phosphatase (ALP), aspartate alanine aminotransferase (ALT), aminotransferase (AST), blood urea nitrogen (BUN) and lactate dehydrogenase (LDH) levels were all within normal range. 8 mice (n=8) were detected for calculation. Data were presented as the mean ± SEM, and were measured by two-tailed unpaired Student' s *t*-test.

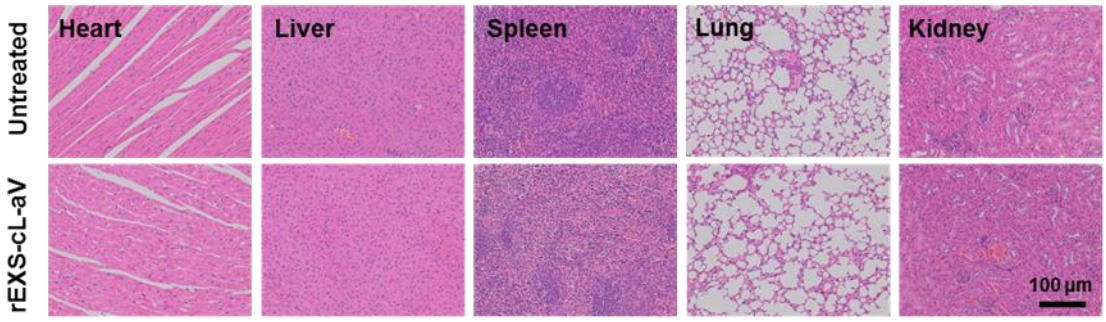

Supplementary Fig. 16. H&E staining of heart, liver, spleen, lung, and kidney slices after treatment with rEXS-cL-aV in a CNV mouse model

rEXS-cL-aV treatment showed no abnormality in above organs.

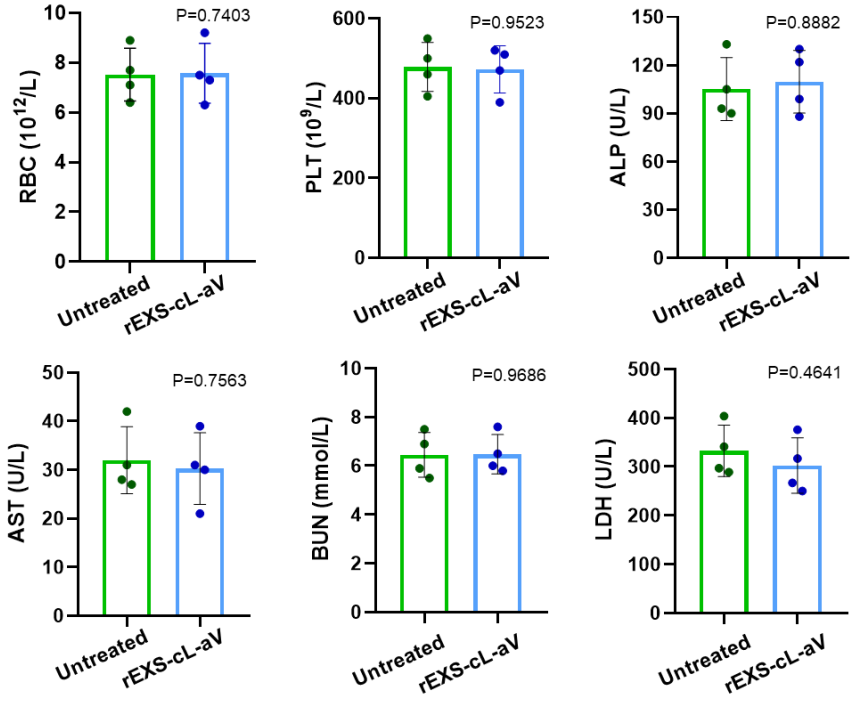

Supplementary Fig. 17. Hematological parameters detection in a CNV monkey model

The red blood cell (RBC), platelet (PLT), alkaline phosphatase (ALP), aminotransferase (AST), blood urea nitrogen (BUN) and lactate dehydrogenase (LDH) levels were all within normal ranges. 4 monkeys (n=4) were detected for calculation. Data were presented as the mean ± SEM, and were measured by two-tailed unpaired Student' s *t*-test.

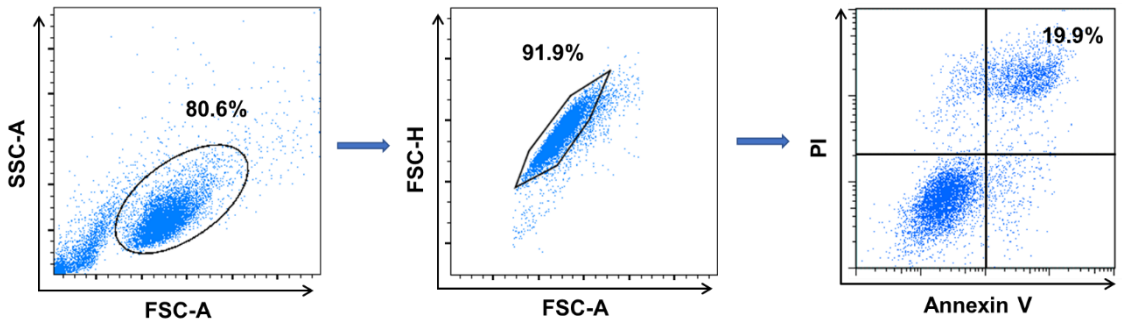

Supplementary Fig. 18. Flow cytometry gating strategy for Fig. 3c

The single cells were identified by FSC and SSC.

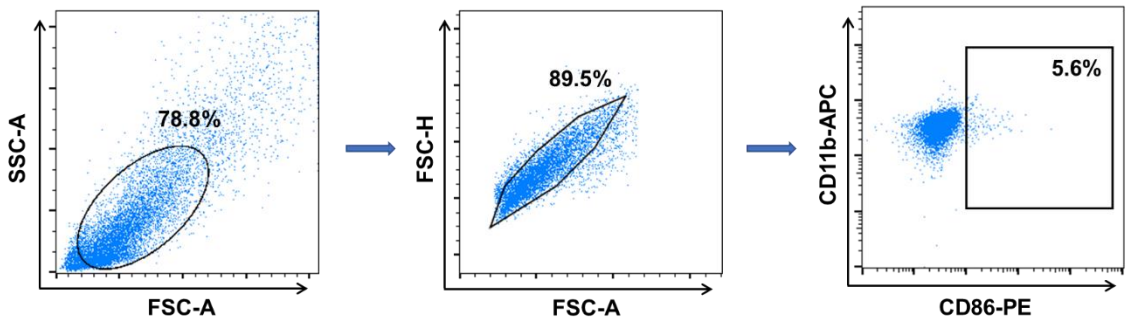

Supplementary Fig. 19. Flow cytometry gating strategy for Fig. 3e

The single cells were identified by FSC and SSC.